Research on Corrosion Fatigue Crack Propagation Behavior of Welded Joints of A7N01P-T4 Aluminum Alloys

J. An[a], J. Chen[a,b], G. Gou[a]*, C. Qin[a], H. Chen[a], P. Li[c], Z. Li[d]

[a]School of Materials Science and Engineering, Southwest Jiaotong University, Chengdu, 610031,

China

[b]Chengdu Industry and Trade College, Chengdu, 611731, China

[c]CSR Qingdao Sifang Co. Ltd, Qingdao,266000, China

[d]Quantum Design China, Beijing, 100027, China

Abstract: Corrosion fatigue failure is one failure form of structure under the service of cyclic load in corrosive environments, but there is little research on the corrosion fatigue property of A7N01P-T4 aluminum alloy and its welded joints, especially the crack propagation behavior. Consequently, the corrosion fatigue crack propagation behavior of welded joints of A7N01P-T4 aluminum alloys were investigated. Microstructures of welded joints were examined by optical microscope (OM), electron back-scattered diffraction (EBSD), μ -X360n portable X-ray residual stress and texture analyzer, and scanning electron microscope (SEM); then the fractures were examined. The potentiodynamic polarization measurement of the joints was studied. The result shows that the propagation rate of corrosion fatigue crack of base metal (BM) was higher than that of the heat-affected zone (HAZ), and the welding seam material (WM) had a better corrosion fatigue resistance. Besides, the second phases had great effect on the corrosion fatigue crack propagation rate of A7N01P-T4 aluminum alloys. The chain-like second phases along the rolling direction were likely to develop into the microcrack under the action of corrosive medium, which would greatly increase the corrosion fatigue crack propagation rate of A7N01P-T4 aluminum alloys.

Keywords: Corrosion Fatigue, Crack Propagation, A7N01P-T4 Aluminum Alloys, Welded joints, Second Phases

1. Introduction

Corrosion fatigue failure is one of the failure forms of structures under the service of cyclic load in corrosive environment. This failure form often occurs in 2xxx and 7xxx series of aluminum alloys of aircraft, vehicles and other important transportation structures and more than half of failures were in correlation with corrosion fatigue. As a result, the corrosion fatigue life of structures is far shorter than that of air fatigue, especially when the applied stress is much closer to the fatigue limit of the structures. There are many factors that affect the corrosion fatigue crack propagation rate of materials, including temperature, PH, concentration of corrosive solution, and so on. M.A. Wahab[1] found that increasing stress ratio has a tendency to have negative effect on fatigue life of 2024-T3 aluminum alloys and the water vapor reduces the fatigue life. U. Zupanc[2] discovered that fatigue resistance of the corrode specimens drastically decreased in comparison with the parent material due to material pitting corrosion. J. Tan found that the cumulative fatigue damage of materials could be divided into the following process [3]: (1) cyclic plastic deformation; (2) micro-cracks nucleation; (3) micro-cracks propagation; and (4) macroscopic cracks propagation. And Li Xu-Dong[4] found the

1

distribution of corrosion pits had a strong effect on the fatigue crack propagation behavior in micro scale and these pits can change the path of fatigue crack propagation. Mala M. Sharma[5] found that pitting corrosion on the sample surface acted as a stress concentrator in alloys and crack initiation sites resulting in fatigue failure were at second phase particles and inclusions. J.F. Li [6]discovered that extended ageing also led to the coarsening and discontinuous distribution of grain boundary precipitates and these two factors contributed the evolution of corrosion mode. Previous results showed that pits would be preferentially formed around the impurities, which had a higher ionization tendency than aluminum substrate and would firstly occur the electrochemical dissolution effect [7] and pits were always ellipsoidal [8]. Besides, the life of aluminum alloys in corrosive solution would be shortened by 2-3 times than that in air [9]. The rising temperature and PH would generally reduce corrosion fatigue strength [10]. The pre-existing interfacial void between oxide film and matrix might promote the formation of $Mg(OH)_2$ corrosion layer, which could provide   temporary protection [11]. Meanwhile, a small number of research has been made about fatigue crack propagation behavior of aluminum alloys welded joints. LIU Xue-song found[12] that the difference of fatigue crack initiation life for base metal, weld metal and HAZ is negligible. The ratio of Ni to Nf is independent on stress amplitude, but dependent on microstructure and mechanical property. R. SEETHARAMAN[13] found that, With the increase in the chloride ion concentration, the corrosion rate of friction stir welded AA2024 aluminum alloy increases in the salt spray corrosion test, but the rising rate of corrosion decreases due to the formation hydroxyl chloride layer. Kalenda Mutombo[14] discovered that corrosion pits appear to be associated with precipitates in the aluminum matrix and act as preferential fatigue crack initiation sites. This reduces the time required for fatigue crack initiation and decreases the total fatigue life.

A7N01P-T4 is a kind of Al-Zn-Mg alloy that has high strength, good extrusion, and good welding properties. Its yield strength and tensile strength can reach to 295MPa, 407MPa respectively, and its elongation can reach to 11.8%. It has been selected to make the welded components of high-speed trains, such as under-frames and other key parts subjected to static and dynamic loading [9]. When aluminum alloys run with loading stress, combined with residual stress in corrosive environments, it is much more sensitive to failure than in the air. Prior research is mostly about fatigue properties of welded joints in air environment, but there is little research on the corrosion fatigue properties of the A7N01P-T4 aluminum alloy and its welded joints, especially the crack propagation behavior.

This paper reports the results from our investigation on corrosion fatigue properties, especially on crack propagation behavior.

2. Materials and Methods

2.1．Materials

The experiment materials are A7N01P-T4 aluminum alloy plates (P stands for plate and T4 stands for a steady state after-solution treatment and natural cooling according to JIS H4000-2006). Welding was performed by the Metal Inter-Gas(MIG) technique with a Transpuls Synergic 4000 welding machine. The welding wires are ER5356 of 1.2mm diameter. The chemical compositions of the A7N01P-T4 Al alloy BM and the welding wire is listed in Table 1. The welding parameters are listed in Table 2. To remove the oxides and reduce the porosity of the joints, the surface of the alloy was chemically cleaned before welding.

Table 1
Chemical composition of BM and welding wire

Material	Zn	Mg	Cu	Mn	Ti	Si	Fe	Cr	Al
A7N01P-T4	4.0~5.0	1.0~1.8	0.10	0.20~0.70	0.01~0.06	0.35	0.40	0.06~0.20	Bal.
ER5356	0.10	4.5~5.5	0.1	0.05~0.20	0.2	0.25	0.10	--	Bal.

Note: 1. The chemical composition of A7N01P-T4 refers to JIS H4000-2006: Temper designation system for wrought aluminum and aluminum alloy. 2. The chemical composition of ER5356, which is similar to filler metal, was listed for future analysis.

Table 2
Welding parameters for the A7N01P aluminum alloy welded joints

Material	Thickness/ mm	Peak current/A	Welding voltage/V	Wire feeding speed/(m/min)	Welding speed/(mm/s)	Note
A7N01 P-T4	8	192	23.2	12	7	Backing welding
		173	22.7	10	8	Cover welding

Note: the gas used for welding is 99.999% purity argon.

2.2．Microstructure observation

The microstructure of welded joints of A7N01P-T4 aluminum alloy were examined by means of Zeiss.A1m optical microscope(OM), electron back-scattered diffraction(EBSD), μ-X360n X-ray residual stress detector and JSM-6490LV scanning electron microscope(SEM). All specimens were mechanically grinded using the different size of metallographic sandpapers from 240 to 2000 grit and were polished on the automatic polishing machines until there were no scratches on the surface of specimens. After polishing, the specimens were cleaned in alcohol and were corroded by Keller's corrosives with a proportion of 2% HF, 3% HCl, 5%HNO$_3$ and 90% H$_2$O. When EBSD was hired, analysis was made to studied the distribution of the second phases. All the specimens were electropolished in electrolyte solution consisting of 10% perch loric acid in 90% ethanol. The electropolishing process ran with a voltage of 25V and polishing time of 38s. A mechanically polished specimen was used to studied the deformation degree of grains of A7N01P-T4 aluminum alloy by μ-X360n. The fracture was observed by means of SEM to study the changes of the second phases during the process of corrosion fatigue crack growth.

2.3. Potentiodynamic polarization measurement

The polarization curve was tested using CHI 660C electrochemical corrosion workshop. The electrochemical testing of specimens was measured by three-electrode system: the specimen itself acted as a working electrode, platinum electrode and saturated calomel electrode were respectively used as anauxiliary electrode and reference electrode. The working area of specimen is 0.45cm^2 and the specimen was polished on the automatic polishing machines. The electrochemical testing medium was 3.5%wt.NaCl. The electrochemical testing was conducted within the scanning potential range of -0.3~0.3 at 25℃, with a scanning rate of 1 mV/s.

2.4. Corrosion Fatigue Cracking Experiment

Corrosion fatigue crack propagation experiment was performed according to ISO 12108: Metallic

materials─Fatigue testing─Fatigue crack growth method. The specimens were improved from single edge notched tension specimen (SENT) in ISO 12108. The specimens of BM and welding joints were machined along Y-X(X stands for the direction paralleling to the welding line and Y stands for the direction perpendicular to the welding line). BM, HAZ and WM respectively stands for the specimen in BM, the heated-affected zone and the welded joint. Sampling method and dimension of corrosion fatigue specimen are shown in Fig.1.
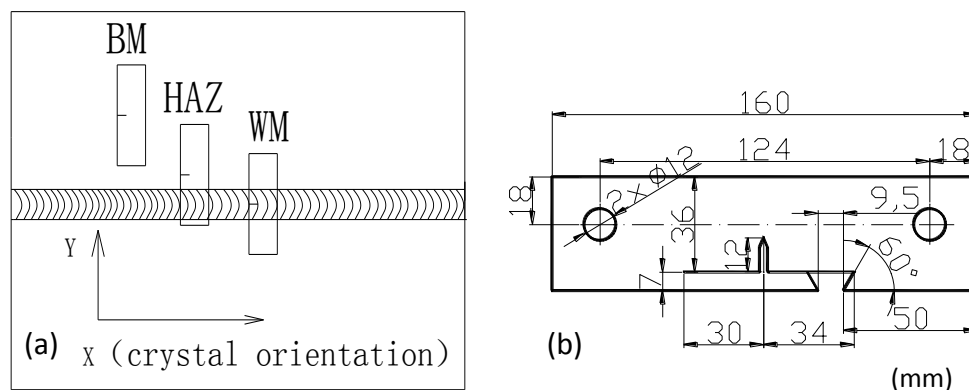
Fig.1 Sampling method and dimension of corrosion fatigue specimen (a) Sampling method (b) dimension of corrosion fatigue specimen

Specimens in the direction of Y-X (shown in Fig.1) for corrosion fatigue cracking experiment were cut and machined from the BM, HAZ and WM of the welded joints according to ISO 12108. A notch was cut at the edge of each specimen in the same way. The pre-setting notch was 2mm long. The pre-crack length was 1-2mm long, which was made by the fatigue testing machine.

To assure the accuracy of the experiment data, only the region of notch was immersed into the solution, and the extensometer was isolated from corrosive solution by a separation board to prevent the extensometer from corroding. A cyanoacrylate adhesive glue was used to prevent leakage. The specimens were clamped in the corrosion solution container made of plexiglass, which allows for observation of the crack growth process due to its transparency. The specimen was clamped on the testing machine through two fixtures which were locked together with specimen by two pins, shown in Fig.2.

The corrosion fatigue experiments were conducted under an alternating load condition with a triangle load wave on a PWS00 servo-hydraulic universal testing machine. Specimens were immersed in 3.5%NaCl solution at the temperature of $25\pm1℃$ and experiments were conducted in a closed laboratory with air conditioning. The crack opening displacement was monitored during the test with an extensometer until the instant break occured. The stress ratio was R=0.1, R=0.2, R=0.3, respectively. Other experiment conditions are listed in Table 3.
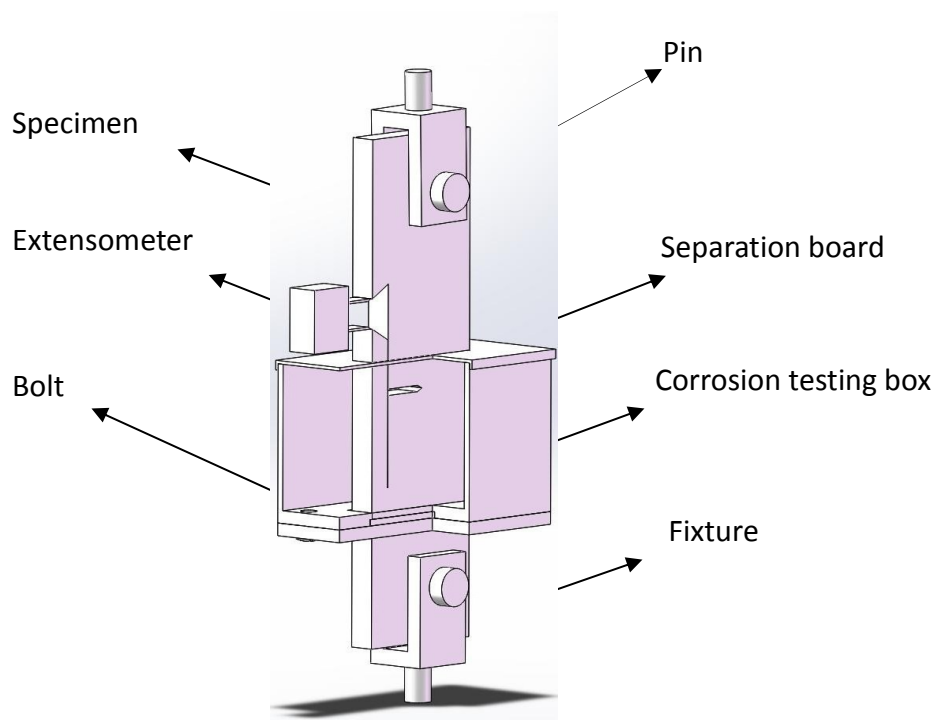
4

Fig.2 Clamping sketch of the specimen

Table 3
Test condition of the different specimens

No.	R	Load amplitude(KN)	Maximum load(KN)	Concentration of NaCl(%)	Frequency (Hz)	Tested area
1	0.1	3.6	4	3.5	0.5	WM
2	0.2	3.6	4.5	3.5	0.5	WM
3	0.3	3.6	5	3.5	0.5	WM
4	0.1	3.6	4	3.5	0.5	HAZ
5	0.2	3.6	4.5	3.5	0.5	HAZ
6	0.3	3.6	5	3.5	0.5	HAZ
7	0.1	3.6	4	3.5	0.5	BM
8	0.2	3.6	4.5	3.5	0.5	BM
9	0.3	3.6	5	3.5	0.5	BM

3. The results and discussion

3.1. Microstructure

   Three directions of microstructures of A7N01P-T4 aluminum alloy were shown in Fig.3. From Fig.3, the grains in X-Y plane were arranged uniformly and had a negligible plastic deformation, while the grains in the Y-Z plane were "squashed." As a result, vimineous grains along the X direction formed. There was also a particularly severe deformation of grains in X-Z plane. From the

5

completeness of the 2D- and 3D- map of the Debye ring and diffraction intensity of Debye ring by μ -X360n portable X-ray residual stress and texture analyzer, grain orientation and distribution could be qualitatively analyzed. The more complete and the lower the diffraction intensity of the Debye ring was, the more uniform the grains were. The results showed that the Debye ring of the X-Y plane was almost complete (2D- and 3D- maps in (a) of Fig.3), the Debye ring of Y-Z plane was complete in part (2D- and 3D- maps in (b) of Fig.3) but the Debye ring was hardly formed in the X-Z plane (2D- and 3D- maps in (c) of Fig.3). The diffraction intensity of the Debye ring in the X-Y plane was at the highest value and up to 928K((a) in Fig.3), the diffraction intensity of the Debye ring in the Y-Z plane was at the medium value and up to 583K((b) in Fig.3) and the diffraction intensity of the Debye ring in the X-Z plane was only 281K. In conclusion, grains of A7N01P-T4 aluminum alloy sharply distorted under the rolling load, and there was great diversity in different directions, which led to different mechanical properties in three different directions.
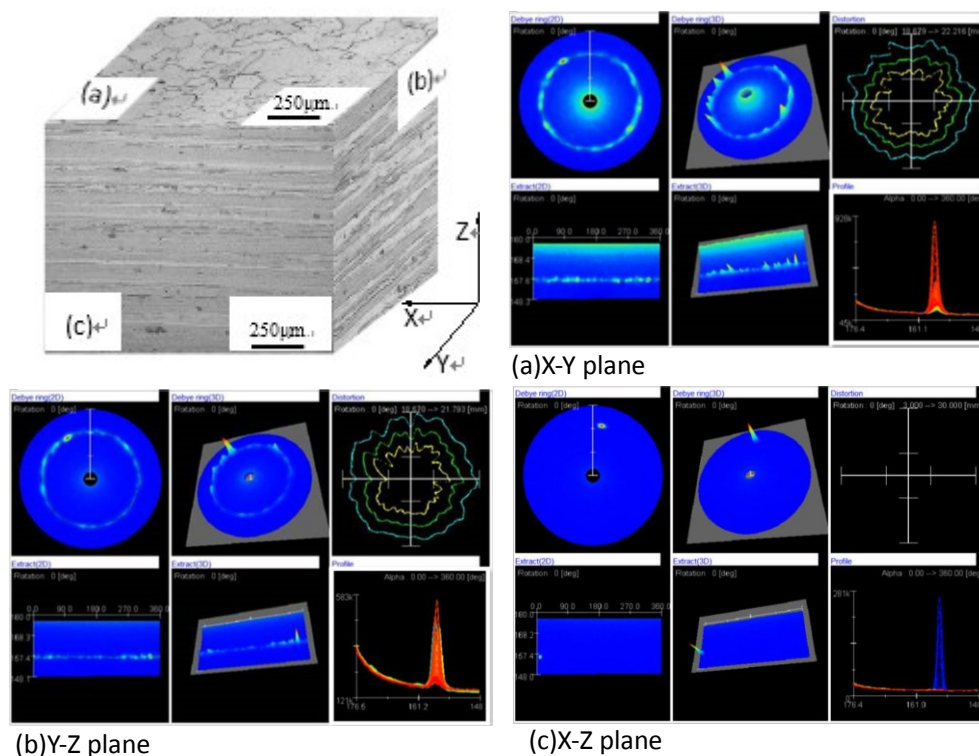

Fig.3 Optical 3D micrographs showing the typical grain structure of A7N01P-T4 aluminum alloy and the test results of grain size by μ -X360n portable X-ray residual stress and texture analyzer: (a) The test result of X-Y plane. (b) The test result of Y-Z plane. (c) The test result of X-Z plane.

The microstructures of welded joints were observed by OM, shown in Fig.4. The same parts of backing welding and cover welding have a similar microstructure. The WM was mainly the mixed structure of dendrites and equiaxed grain (Fig.4 a, b). The microstructure close to the WM consisted of fine equiaxed grain (Fig.4 c, d), while the microstructure close to the HAZ was mainly coarse grains (Fig.4. c, d). The grains of the HAZ had a distinct preferred direction along the rolling

6

direction (Fig.4 e, f). However, the deformation of the HAZ was less than that of BM (Fig.3) because recovery and recrystallization of A7N01P-T4 aluminum alloy had occurred during the welding.
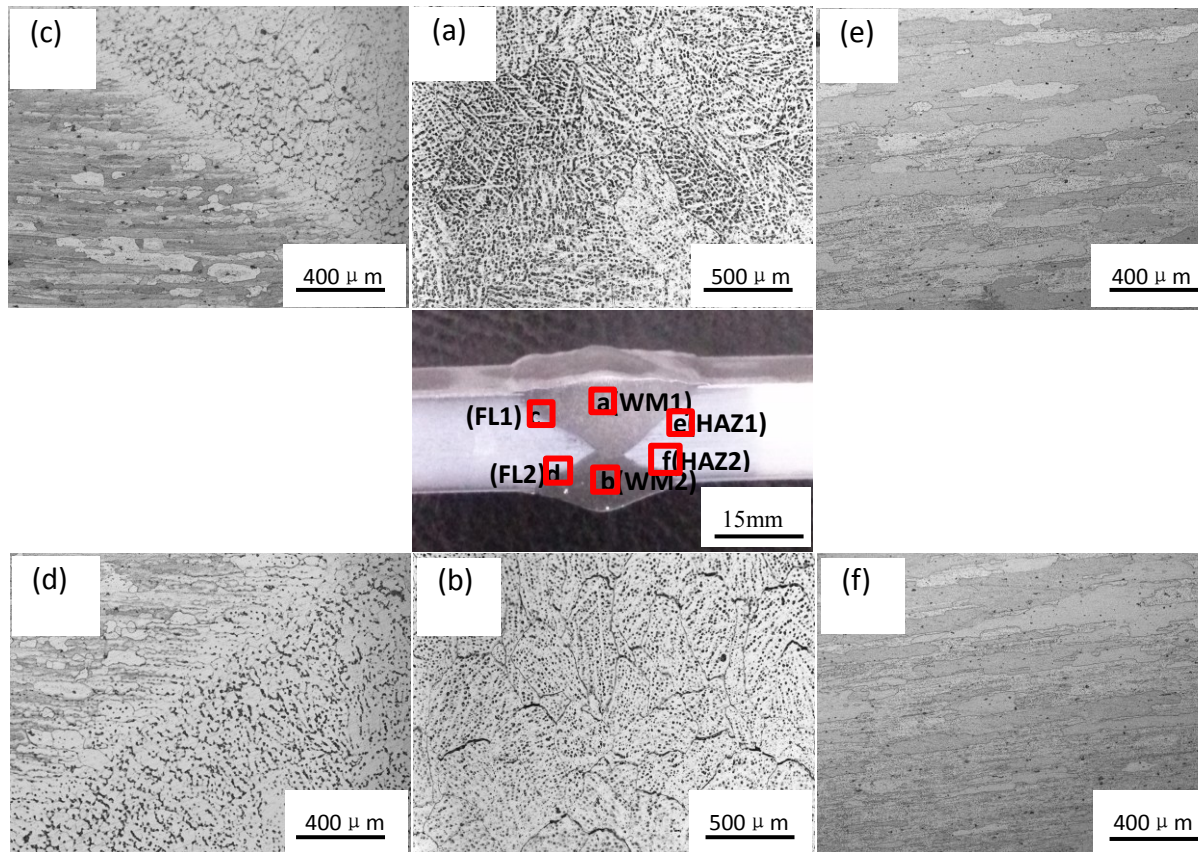

Fig.4 The microstructure of welded joints: (a) the microstructure of WM of cover welding, (b) the microstructure of WM of backing welding, (c) the microstructure of fusion line of cover welding, (d) the microstructure of fusion line of cover welding, (e) the microstructure of the HAZ of cover welding, (f) the microstructure of the HAZ of backing welding.

3.2． Corrosion Fatigue Crack Propagation Rate Experiment

The relationship of corrosion fatigue crack propagation rate da/dN vs. stress intensity range △K were shown in Fig.5. In order to get the statistics disciplinarian and trend disciplinarian, the seven points incremental polynomial method was used. The Paris equation (1) was used to process the measured data.

$$\frac{da}{dN} = C \times \Delta K^m \qquad （1）$$

Where da/dN is the fatigue crack propagation rate; △K is the stress intensity range; C, m are the material constants.
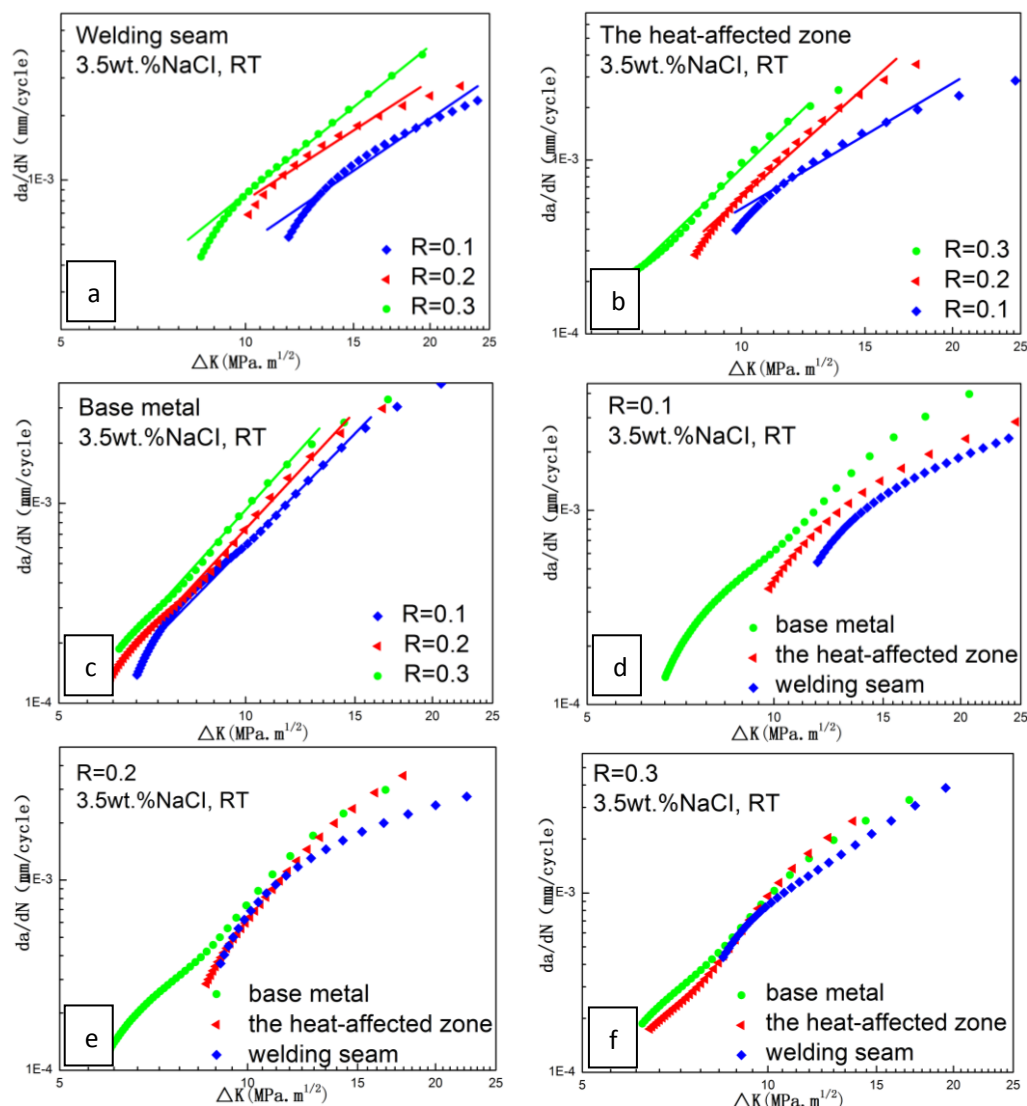
7

Fig.5 da/dN versus △K curves of BM and welded joints: (a) corrosion fatigue crack propagation rate (CFCGR) curves of WM under different stress ratio, (b) CFCGR curves of the heat-affected zone under different stress ratio, (c) CFCGR curves of BM under different stress ratio, (d) CFCGR curves of WM, the heat-affected zone and BM under stress ratio R=0.1, (e) CFCGR curves of WM, the heat-affected zone and BM under stress ratio R=0.2, (f) CFCGR curves of WM, the heat-affected zone and BM under stress ratio R=0.3.

From the results, the propagation rate of corrosion fatigue crack of BM, the HAZ and WM increased with the increase of stress ratio R (Fig.5). Under the same stress ratio, the propagation rate of BM was the highest, the propagation rate of HAZ was the medium and the WM was the lowest (d, e and f in Fig.5). The microstructures of the fractured welded joints were shown in Fig.6.
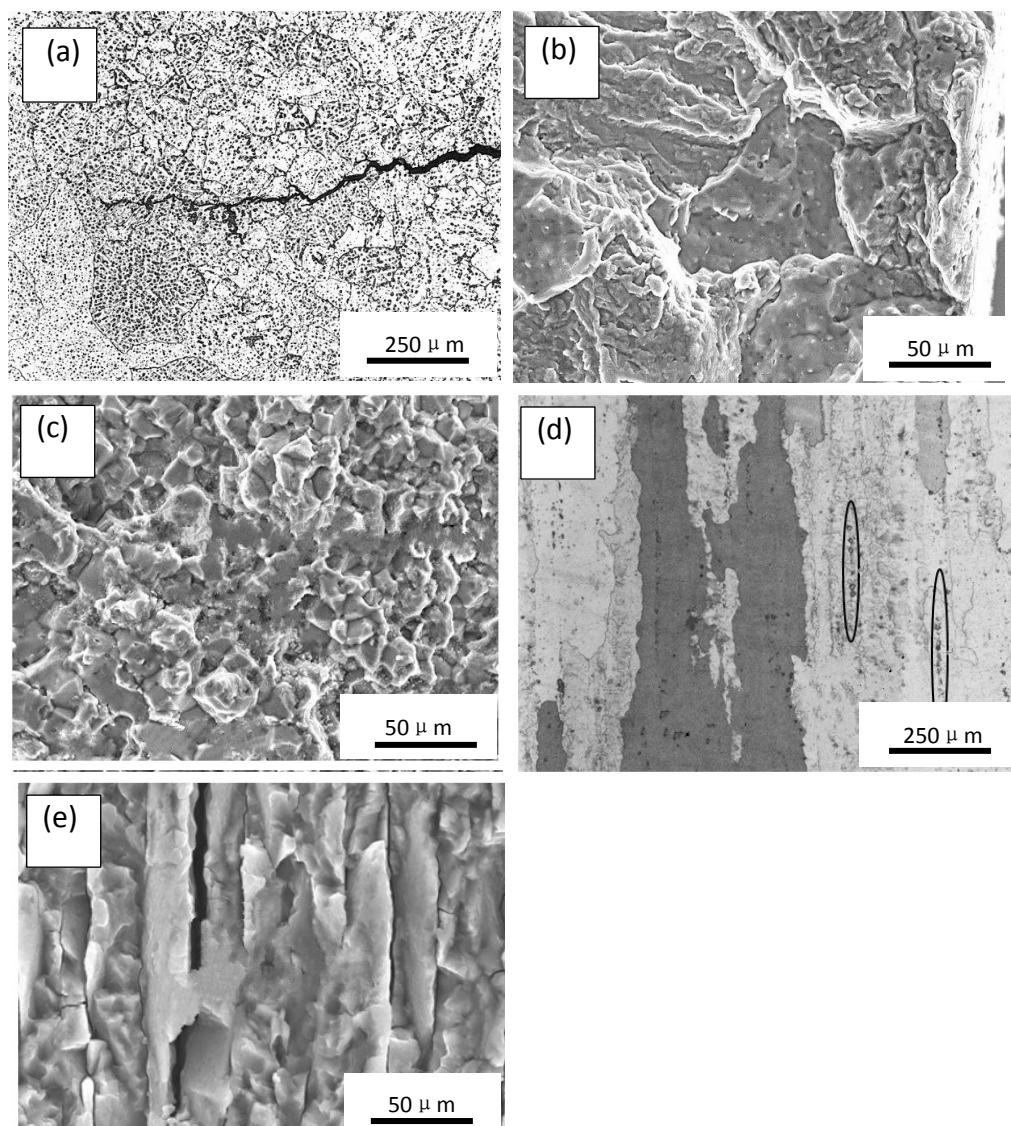
8

Fig.6 metallographic structure and fracture surface of welded joints: (a)The crack propagation path of the WM under the OM, (b) transgranular fracture of the WM by SEM, (c) intergranular fracture of the WM by SEM, (d) microstructure of the HAZ under the OM, (e) the secondary crack of the HAZ by SEM.

It can be seen that the crystallizing morphology of the WM is equiaxed grains and the fracture model is predominantly transgranular, accompanied with small amounts of intergranular cracking (Fig.6. (a), (b) and (c)). Because of high content of magnesium in ER5356 welding wire (Table 1), the precipitates in WM are magnesium-rich. The precipitates in the HAZ are mainly the zinc-rich. Due to the polarization curves (Fig.7), the HAZ has a higher corrosion current density of 1.09×10^{-6} Amps/cm^2, compared to that of WM, which is 1.78×10^{-8} Amps/cm^2. Besides, the grains of the HAZ are coarser than that of WM (Fig.6. (d)). The long,continuous grain boundary of the WM acts as a channel for corrosion fatigue crack propagation and secondary cracks are easy to be formed

9

along the grain boundary (Fig.6. (e)). As a result, the WM has a greater resistance to corrosion fatigue cracking than the WM.
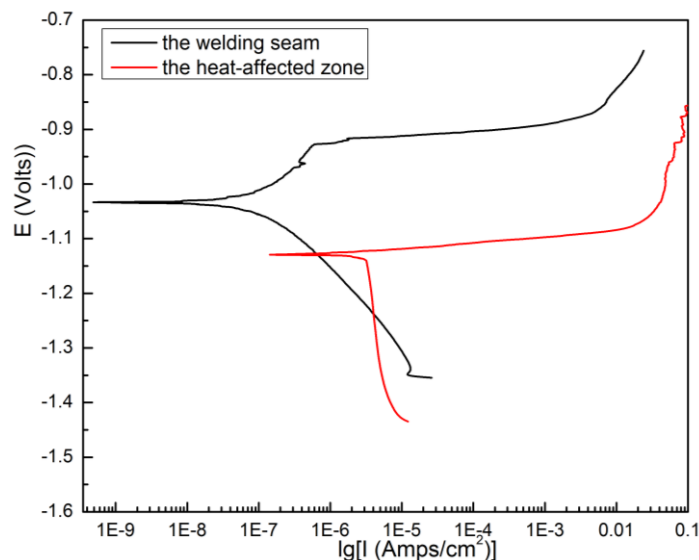

Fig.7 Polarization curves of the welding seam(WM) and the heat-affected zone(HAZ)
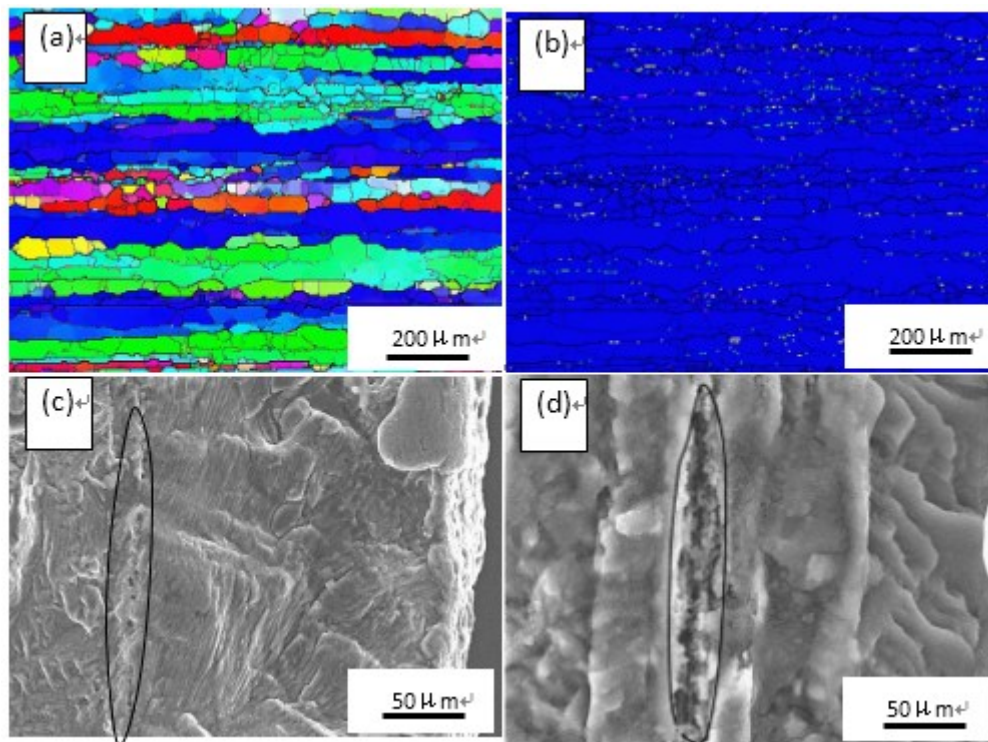

Fig.8. Microstructure of the BM by SEM and EBSD: (a) the rolling structures of BM by EBSD, (b) secondary phase distributed along crystal boundary of BM by EBSD. (c) chain-like corrosion pits and fatigue striations on the fracture of BM by SEM, (d) tiny crack on the fracture of BM by SEM.

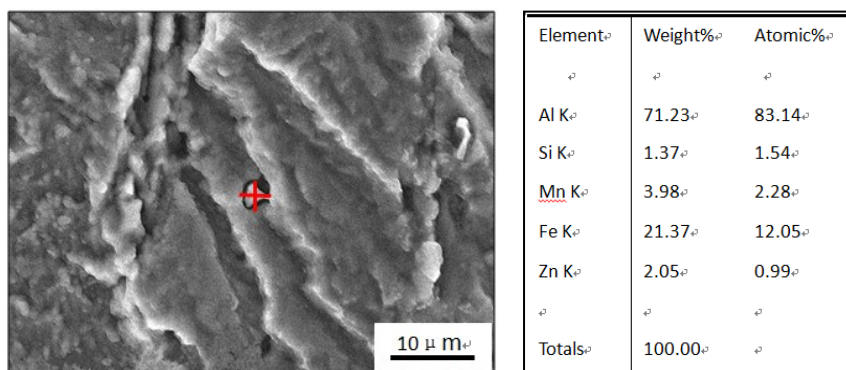| Element	Weight%	Atomic%
Al K	71.23	83.14
Si K	1.37	1.54
Mn K	3.98	2.28
Fe K	21.37	12.05
Zn K	2.05	0.99
Totals	100.00	

Fig.9 Component analysis of the second phases

The microstructures of BM were typical rolling structures and the second phases were uniformly arranged in chain-like formations on the grain boundaries (Fig.8 (a), (b)). From the result of component analysis(Fig.9), the second particle was rich in Fe, which was one of the most common impurities in industrial aluminum. Fe would inevitably unite with the matrix and form some impurities like $FeAl_3$, $Al_{4.5}FeSi$ and Al_3Fe_2Si. From Fig.11d, A7N01P-T4 aluminum alloy is rich in Fe, which enriched at the grain boundaries. Those impurities were hard, as well as brittle. The stress concentrate can be formed in some places where the impurities existed. As a result, second phases would easily break or separate from the matrix, which lead to the forming of cracks[15, 16] and greatly affected the localized corrosion behavior of Al alloys. The corrosion model of the second phases is shown in Fig.10. At the early stage, Al and Fe would be dissolved and form $Al(OH)_3$ and Fe^{2+}. Then the corrosion pits were formed. Furthermore, with the negative shift of potential, Fe^{2+} would partly deposit in the corrosion pits, and the rest forms into $Fe(OH)_2$ out of the corrosion pits, which would tightly wrap the $FeAl_3$, together with $Al(OH)_3$. As a result, $FeAl_3$ was protected from further dissolution. On the other hand, the hydrogen evolution reaction occurred in the corrosion pits, thereby promoting the anodic dissolution of aluminum substrate in the corrosion pits. The reaction could be summarized as follows: $2H^+ + 2e \rightarrow H_2$(cathode); $Al \rightarrow Al^{3+} + 3e$(anode).

After the separation of second phases from the matrix, corrosion pits were formed and arranged in chain-like formations on the fracture surface, and some of them even formed a continuous line that could be considered a tiny crack (Fig.8 (c), (d)), which would greatly accelerate the corrosion fatigue crack propagation of A7N01P-T4. So it is very necessary to avoid the introduction of impurity elements like Fe during the manufacturing process.

The microstructure of the boundary between BM and the WM in X-Y plane (Fig.3) is shown in Fig.11. The BM and the WM are divided into two parts with a clear line (Fig.11 (a)), which turns out to be the continuously arranged second phases at high magnification (Fig.11 (b)). Under the influence of the welding thermal cycle, the microstructures in HAZ become coarser. The second phases were partly redissolved into the matrix in the process of welding. At the same time, the second phases that had not dissolved into the matrix were pushed, with the expansion of the grain boundary, into the areas near the BM. Therefore, the second phases arranged near the boundary between BM and the WM were dense (Fig.11 (c), (d)). As a result, the WM had fewer second phases

and was less likely to form the corrosion pits. In conclusion, the WM had better resistance to corrosion fatigue cracking than BM.

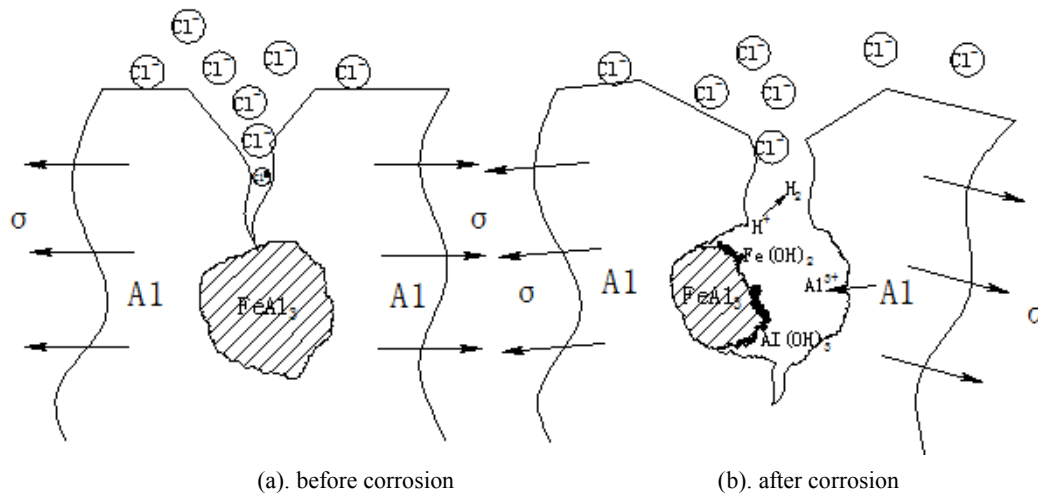(a). before corrosion　　　　　　　　　　(b). after corrosion

Fig.10 The Corrosion Model of the Second Phases: (a) before corrosion, (b) after corrosion
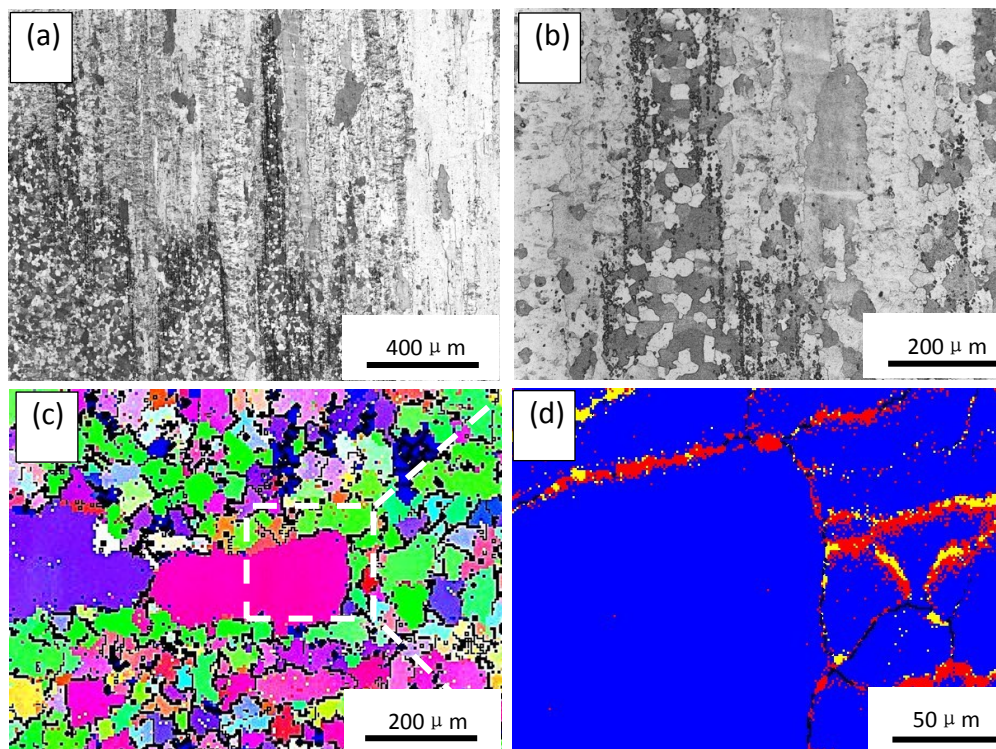

Fig.11. Microstructure of the boundary between BM and the WM by SEM and EBSD: (a)OM microstructure of the boundary between BM and the WM at low magnification, (b)OM microstructure of the boundary between BM and the WM at high magnification, (c)EBSD microstructure of the boundary between BM and the WM at low magnification, (d) EBSD microstructure of the boundary between BM and the WM at high magnification(the second phases in red were rich in Fe and the second phases in yellow were other second phases without Fe).

12

4. Conclusion

The behavior of corrosion fatigue-crack propagation of BM and welded joints of A7N01P-T4 aluminum alloy in 3.5%wt.NaCl under the different stress ratio was studied in this paper. On the basis of the test results, the conclusions are drawn as follows:

(1) A7N01P-T4 aluminum alloy had a rolling structure. The grains were elongated along the rolling direction and the microstructure in three directions were different from each other.

(2) The WM of A7N01P-T4 aluminum alloy had a better corrosion fatigue resistance than that of the WM in 3.5%wt.NaCl, and BM had the worst corrosion fatigue-resistant performance.

(3) The second phases in A7N01P-T4 aluminum alloy were rich in Fe and were distributed mainly along the grain boundary. Chain-like second phases led to the formation of microcracks during the process of corrosion fatigue crack propagation, which greatly reduced the corrosion fatigue-resistant performance of A7N01P-T4 aluminum alloy. So it is very necessary to avoid the introduction of impurity elements like Fe during the manufacturing process.

References：

1. M. Wahab, J. Park, M. Alam, and S. Pang: 'Effect of corrosion prevention compounds on fatigue life in 2024-T3 aluminum alloy', *Journal of materials processing technology*, 2006, **174**(1), 211-217.

2. U. Zupanc and J. Grum: 'Effect of pitting corrosion on fatigue performance of shot-peened aluminium alloy 7075-T651', *Journal of Materials Processing Technology*, 2010, **210**(9), 1197-1202.

3. W. Shuo1a, C. Xu1a, Y. Kai, X. Wei, and F. Fei1b: 'The simulation and experimentation study of fatigue crack propagation of aluminum alloy under corrosion enviroment [J]', *Journal of Shenyang Aerospace University*, 2013, **2**, 018.

4. X.-D. Li, X.-S. Wang, H.-H. Ren, Y.-L. Chen, and Z.-T. Mu: 'Effect of prior corrosion state on the fatigue small cracking behaviour of 6151-T6 aluminum alloy', *Corrosion Science*, 2012, **55**, 26-33.

5. M. M. Sharma, J. D. Tomedi, and J. M. Parks: 'A microscopic study on the corrosion fatigue of ultra-fine grained and conventional Al–Mg alloy', *Corrosion Science*, 2015, **93**, 180-190.

6. J. Li, N. Birbilis, D. Liu, Y. Chen, X. Zhang, and C. Cai: 'Intergranular corrosion of Zn-free and Zn-microalloyed Al–xCu–yLi alloys', *Corrosion Science*, 2016.

7.   S. Ishihara, Z. Nan, A. McEvily, T. Goshima, and S. Sunada: 'On the initiation and growth behavior of corrosion pits during corrosion fatigue process of industrial pure aluminum', *International Journal of Fatigue*, 2008, **30**(9), 1659-1668.

8.   D. Harlow and R. Wei: 'A probability model for the growth of corrosion pits in aluminum alloys induced by constituent particles', *Engineering Fracture Mechanics*, 1998, **59**(3), 305-325.

9.   P. Pao, S. Gill, and C. Feng: 'On fatigue crack initiation from corrosion pits in 7075-T7351 aluminum alloy', *Scripta Materialia*, 2000, **43**(5), 391-396.

10.   D. J. DUQUETTE: 'Corrosion fatigue', *Corrosion Mechanisms*, 1986, **28**, 367.

11.   W. Yang, Z. Zhu, J. Wang, Y. Wu, T. Zhai, and G.-L. Song: 'Slow positron beam study of corrosion behavior of AM60B magnesium alloy in NaCl solution', *Corrosion Science*, 2016, **106**, 271-280.

12.   X.-s. LIU, L. ZHANG, L.-s. WANG, S.-h. WU, and H.-y. FANG: 'Fatigue behavior and life prediction of A7N01 aluminium alloy welded joint', *Transactions of Nonferrous Metals Society of China*, 2012, **22**(12), 2930-2936.

13.   R. Seetharaman, V. Ravisankar, and V. Balasubramanian: 'Corrosion performance of friction stir welded AA2024 aluminium alloy under salt fog conditions', *Transactions of Nonferrous Metals Society of China*, 2015, **25**(5), 1427-1438.

14.   K. Mutombo and M. Du Toit: 'Corrosion fatigue behaviour of aluminium alloy 6061-T651 welded using fully automatic gas metal arc welding and ER5183 filler alloy', *International Journal of Fatigue*, 2011, **33**(12), 1539-1547.

15.   K. Ma, H. Wen, T. Hu, T. D. Topping, D. Isheim, D. N. Seidman, E. J. Lavernia, and J. M. Schoenung: 'Mechanical behavior and strengthening mechanisms in ultrafine grain precipitation-strengthened aluminum alloy', *Acta Materialia*, 2014, **62**, 141-155.

16.   Ø. Ryen, B. Holmedal, O. Nijs, E. Nes, E. Sjölander, and H.-E. Ekström: 'Strengthening mechanisms in solid solution aluminum alloys', *Metallurgical and Materials Transactions A*, 2006, **37**(6), 1999-2006.